RSC Advances

PAPER

View Article Online
View Journal | View Issue

Cite this: *RSC Adv.*, 2025, **15**, 2996

Novel mixed matrix membranes with indium-based 2D and 3D MOFs as fillers and polysulfone for CO_2/CH_4 mixed gas separation†

Aditya Jonnalagedda and Bhanu Vardhan Reddy Kuncharam *

To address the limitations of polymeric membranes, mixed matrix membranes for CO_2 separation from biogas mixtures (CO_2 and CH_4) have been investigated utilizing various fillers. In this study, we investigated novel MMMs using 3D and 2D indium-based MOFs, MIL-68(In)–NH_2 and In(aip)$_2$, in a polysulfone polymer matrix. To confirm synthesis, both fillers were subjected to XRD and FTIR analysis, as well as FESEM characterization to assess their 2D and 3D structures. BET analysis revealed the pore size of MOFs. MMMs were characterized using XRD, FTIR, FESEM, and DSC to determine various membrane characteristics. MMMs were tested with CO_2 : CH_4 of 60 : 40 vol% to mimic the biogas mixture, and the CO_2 permeability of 144 Barrer and 79.2 Barrer was obtained for 20 wt% In(aip)$_2$/PSF membrane and 15 wt% MIL-68(In)–NH_2/PSF membrane. The highest CO_2/CH_4 selectivities of 19.8 and 24.4 were obtained for 15 wt% MIL-68(In)–NH_2/PSF MMM and 10 wt% In(aip)$_2$/PSF MMM, respectively. The gas permeation findings of this study were compared with existing literature and long-term stability analysis was done to assess the performance of membranes for commercial standards.

Received 4th December 2024
Accepted 18th January 2025

DOI: 10.1039/d4ra08557d

rsc.li/rsc-advances

1 Introduction

CO_2 (carbon dioxide) emissions have become one of the major causes of global warming, and studies have shown that a decrease in CO_2 emissions can stabilize the earth's surface temperature on multi-century timescales.[1] The main reason for the increase in CO_2 emission is due to the accelerated use of fossil fuels to satisfy the energy demand.[2] To suppress the use of fossil fuels and to satisfy the increasing energy demand, alternative energy sources that are renewable, sustainable, and environmentally friendly need to be explored. Biogas is one of the energy sources obtained by anaerobic digestion of biomass and can be utilized in internal combustion engines as feed.[3]

Biogas composition majorly consists of 60% of CH_4 (methane), 40% of CO_2, and trace amounts of N_2 (nitrogen), H_2O (water vapour) and H_2S (hydrogen sulphide).[4] To enhance the quality of biogas and meet the pipeline specification for the transport of biogas, purification methods such as absorption, adsorption (Pressure Swing Adsorption – PSA), cryogenic separation, and membrane separation are required for the removal of CO_2. Separation techniques such as absorption, PSA, and cryogenic separation incur high solvent, high pressure, and high-power costs (due to the low-temperature process), respectively, which leads to high capital and maintenance costs. On the other hand, due to its rapid advancement, membrane technology can offer cost-effective and energy-efficient separation methods.[5,6] In the membrane separation technique, inorganic and polymeric membranes are employed for the separation of CO_2/CH_4 (ref. 7) but have limitations of high fabrication cost (for inorganic membranes) despite the high separation performance of CO_2/CH_4 (ref. 8) and low selectivity and plasticization (for polymeric membranes).[9] Mixed matrix membranes (MMMs), a combination of polymeric and inorganic membranes, are introduced to overcome the above-mentioned limitations. In MMMs, many factors need to be addressed, such as novel fillers in polymer and their interaction, polymer rigidification at the filler–polymer interface, and filler agglomerations at higher loadings.[7] To overcome the mentioned hurdles, two dimensional (2D) and three-dimensional (3D) fillers have amine (–NH_2) groups to decrease the filler agglomeration and to improve the filler–polymer interface traditional fillers such as metal organic frameworks (MOFs), covalent organic frameworks (COFs), zeolites, silica, *etc.*, come under the 3D fillers category, and 2D fillers include graphene oxide (GO), MoS_2, MXene, 2D-MOFs, and COFs.[10] MOFs can be both 2D and 3D depending on the synthesis method, linker, and many other factors. MOFs are metal ions bonded with organic ligands, where there are many sub-classes such as Zeolite Imidazolate Frameworks (ZIFs), MILs (Materials Institute Lavoisier), University of Oslo (UiOs) *etc.*, MILs-based MOFs are mostly 3D structures and were first made by Férey[11] by combining metals (Al, Cr, Ti, In, V and Ga) with carboxylate

a, Department of Chemical Engineering, Birla Institute of Technology & Science, Pilani Campus, Pilani, Rajasthan, 333031, India. E-mail: bhanu.vardhan@pilani.bits-pilani.ac.in; Tel: +91-1596255839

† Electronic supplementary information (ESI) available. See DOI: https://doi.org/10.1039/d4ra08557d

ligands.[12] MIL-68(In) and MIL-68(In)-NH_2 MOFs were used in hydrogen (H_2) and carbon dioxide (CO_2) adsorption studies[13] and photocatalysis,[14] the NH_2 group in MOFs was used to enhance CO_2/CH_4 separation where MIL-68(In)–NH_2 MOFs CO_2 uptake value of 1.6 mmol g^{-1} (1.01 Bar, 25 °C),[15] and the gas separation mechanism of MIL-68(In)-NH_2 MOF based MMMs is shown in Fig. 1a. In(aip)$_2$ is an indium-based 2D-MOF with a pore aperture size of 3.4 Å and has the capacity for molecular sieving separation of CO_2 and CH_4 (which can be seen Fig. 1b), and also amine groups which undergo MOF-coordination and also H-bonding and forming Brønsted basic sites which improve the CO_2 affinity, and CO_2 uptake of 1.27 mmol g^{-1} and selectivity of 1808 and 2635 were found for CO_2/CH_4 and CO_2/N_2 respectively, at 25 °C and 1.01 bar.[16] Various simulation and experimental studies (for CO_2 adsorption) have been done on pore engineering of MOFs,[17,18] which proved to be good material for CO_2 separation.

MIL-125 was the earlier MIL-based MOF we could find that has been used as a filler in MMMs; MIL-125 (Ti) and MIL-125(Ti)–NH_2 were dispersed in Matrimid polymer, and membranes were fabricated and tested for pure gas at 1 bar and 25 °C. At 30 wt% of filler loading permeability of CO_2 was found to be 50 Barrer for MIL-125(Ti)–NH_2 and 27 Barrer for MIL-125(Ti), whereas selectivity of CO_2/CH_4 remained at 37 for both MMMs.[19] A comparison study was done using synthesized ODPA–TMPDA (ODPA = 4,4′-oxydiphthalic anhydride; TMPDA = 2,4,6-trimethyl-*m*-phenylenediamine) polymer-based MMMs with 2D (ns-CuBDC, ns: nano sheets) and 3D (ZIF-8) MOFs. The prepared MMMs were tested with a binary gas mixture of CO_2 and CH_4. At 2 wt% of ns-CuBDC/ODPA-TMPD, CO_2 permeability was 99 Barrer, and CO_2/CH_4 selectivity of 43, at 10 wt% ZIF-8/ODPA-TMPD 144 Barrer of CO_2 permeability and CO_2/CH_4 selectivity 37.[20] 2D-Ni-based MOF (α-Ni(im)$_2$) were dispersed in Pebax MH-1657 to enhance the separation of CO_2/CH_4 and tested for binary gas mixture of CO_2 and CH_4 at 2 bar pressure, for 2 wt% α-Ni(im)$_2$/Pebax MMM showed CO_2 permeability of 100.6 Barrer and CO_2/CH_4 selectivity of 33.4.[21] The synergistic effect of MXene 2D-nanosheets and 3D UiO-66 nanoparticles in Pebax-1657 polymer was found by fabricating MMMs and tested with mixed gas for CO_2/N_2 separation. At 10 wt% UiO-66-MXene/Pebax-1657 CO_2 permeability and CO_2/N_2 selectivity of 200 Barrer and 100, respectively.[22] Ni-based MOF with naphthalene tetrazole-based linker (Ni-NDTZ) was used as a filler in polycarbonate (PC) polymer to prepare MMMs for CO_2 separation studies and tested with pure CO_2 and CH_4 gases at 1 bar pressure. At 20 wt% Ni-NDTZ/PC MMM the CO_2 permeability was found to be 45 Barrer and CO_2/CH_4 selectivity of 23.7.[23] Thin films MMMs were fabricated with N_2 doped GO (N-GO) in polyimide polymer (PI) and tested pure CO_2 and CH_4 at 3 bar. At 0.02 wt% filler loading of N-GO, CO_2 permeance was 28 GPU and CO_2/CH_4 selectivity of 47.[24] 2D covalent triazene framework (CTF-fullerene) is used as porous filler material for the preparation of MMMs with Matrimid and polysulfone (PSF) polymers and tested with binary gas mixtures of CO_2/CH_4. At 24 wt% of CTF- fullerene in Matrimid and PSF, CO_2 permeability was 12.8 Barrer and 17.8 Barrer, respectively. At the same filler loading, CO_2/CH_4 selectivity of 44 and 30 for Matrimid and PSF MMMs, respectively.[25] Ionic liquid-modified 2D zeolite SAPO-34 (IL@SAPO-34) particles are dispersed in the PSF polymer matrix to fabricate MMMs to study CO_2 separation by testing with single CO_2 and CH_4 gases at 2.75 bar feed pressure. 5 wt% IL@SAPO-34/PSF MMM exhibited CO_2 permeance of 7.24 GPU and CO_2/CH_4 selectivity of 20.4.[26] Indium based MOF of MIL-68(In)–NH_2 was dispersed in PES polymer and tested for pure CO_2, CH_4 and H_2 gases at 60 °C for H_2/CO_2, H_2/CH_4 and CH_4/CO_2 separations. The H_2 and CO_2 permeances were found to be 427 075 and 124 656 Barrer, respectively, at 10 wt% of MIL-68(In)–NH_2. Selectivity of H_2/CO_2 and CH_4/CO_2 were found to be 4 and 1.7.[27]

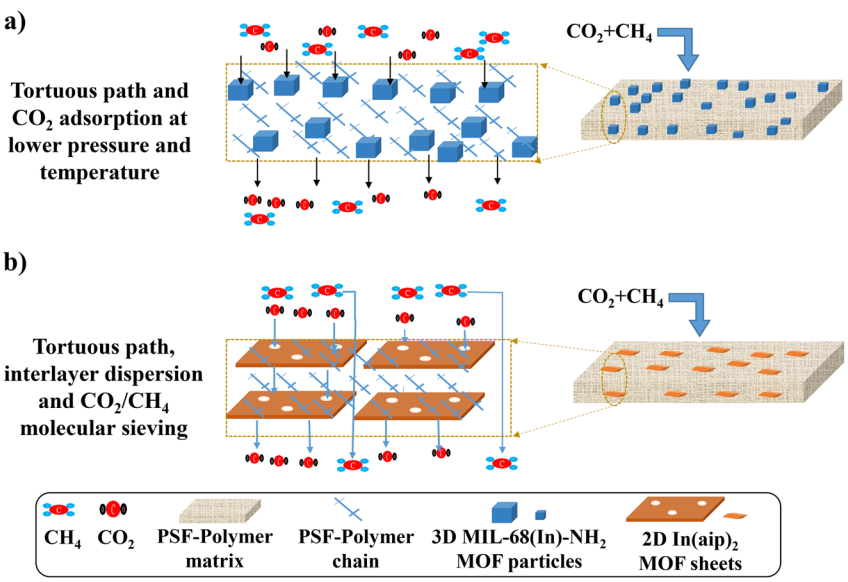

Fig. 1 Illustration of gas separation mechanisms for MMMs in this study, (a) MMM with MIL-68(In)-NH_2 filler and (b) MMM with In(aip)$_2$ filler.

Based on the literature survey we can see that both 3D MOFs and 2D MOFs have improved CO_2 permeation and selectivity due to interlayer spacing and tortuous paths. To our knowledge, we have not found studies with 2D-indium MOF In(aip)$_2$ as a filler in MMMs, and also only one study with MIL-68(In)–NH_2 as a filler in MMMs for CO_2/CH_4 separation. To address this research gaps, in this paper, novel mixed matrix membranes were prepared with synthesized microporous MIL-68(In)–NH_2 and mesoporous In(aip)$_2$ as filler in PSF polymer. The fabricated MMMs are tested for mixed gas of $CO_2 : CH_4$ (of 60% : 40%), which was used to mimic model biogas. A comparison study was conducted for both filler-based MMMs, using their characterization and gas permeation tests.

2 Materials and methods

2.1 Materials

Indium nitrate was purchased from Sisco Research Laboratories (SRL) Pvt. Ltd. 2-Aminoterpthalic acid and 5-aminoisopthlahlic acid were purchased from Sigma Aldrich. Polysulfone (PSF) polymer beads were Tech Inc Membrane Research-India. The solvents, such as methanol (CH_3OH) and ethanol (C_2H_5OH), were procured from Merck Life Science Private Ltd-India, and dimethyl formamide (DMF) from Rankem Chemicals-India. CO_2/CH_4 – mixed gas used for the gas permeation tests was procured from Ankur Speciality Gases and Technologies Private Ltd, Jaipur-India.

2.2 Synthesis of MIL-68(In)–NH_2

MIL-68(In)–NH_2 was prepared using solvothermal synthesis *via* the procedure mentioned in the literature.[14] 1.152 g of indium nitrate was dissolved in 30 ml of DMF, and 0.234 g of 2-aminoterpthalic acid was dissolved in 30 DMF. After dissolving the salt and linker separately, they are combined in a 100 ml Teflon liner and stirred for 15 minutes. The reaction mixture is then sealed in a stainless-steel autoclave and heated at 125 °C for 6 hours; after cooling, the mixture is centrifuged at 7000 rpm for 5 minutes and washed with methanol 3–4 times until the supernatant turns colorless. The wet mixture was dried at 70 °C overnight and then in a vacuum oven at 100 °C for the removal of trace amounts of solvent.

2.3 Synthesis of In(aip)$_2$

Synthesis of In(aip)$_2$ was done by using previous literature,[16] with slight modification. 0.36 g of 2-aminoiospthlahlic acid was dissolved in a mixture of 30 ml of DMF and 10 ml of ethanol, and 0.19 g of indium nitrate was dissolved in 10 ml of deionized (DI) water. Both solution mixtures were combined in 100 ml Teflon liner and stirred for 30 minutes. The Teflon liner was then sealed in a stainless-steel autoclave and heated at 110 °C for 72 hours. After cooling, it is then centrifuged and washed with methanol using the same process as previously mentioned in the synthesis of MIL-68(In)–NH_2.

2.4 Membrane fabrication

The pure polysulfone (PSF) membrane fabrication procedure was mentioned in our previous study.[28] To synthesize MMMs with indium-based MOF fillers- MIL-68(In)–NH_2 and In(aip)$_2$, a predetermined amount of filler (using eqn (1)) was dissolved in 15 ml of chloroform and sonicated for 1 h. 3 g of PSF beads was added to the sonicated MOF solution using the priming technique. The solution mixture was stirred overnight and sonicated for 3 hours with 30 minute cycles. The dope solution mixture was cast on a flat Petri dish and dried overnight at room temperature. To remove the residual solvent, the membranes were dried at 60 °C in a vacuum oven for 6 hours.

$$\text{Filler\% loading} = \frac{\text{weight of the MIL-68(In)} - \text{NH}_2 \text{ or In(aip)}_2}{\text{weight of the MIL-68(In)} - \text{NH}_2 \text{ or In(aip)}_2 + \text{ weight of the PSF}} \quad (1)$$

2.5 Characterizations and gas permeation tests

XRD (X-ray diffraction) analysis was done for MMMs and MOFs – MIL-68(In)–NH_2 and In(aip)$_2$ using Rigaku Miniflex X-ray diffractometer using Cu-Kα radiation with $\lambda = 1.54$ Å, to confirm the crystalline structure of MOFs and analyze the phase change in pure PSF membrane and MMMs. Fourier Transform Infrared (FTIR) of MOFs and MMMs was done to confirm the chemical bonding present in the samples, using PerkinElmer Frontier Spectrometer, where samples were prepared using KBr press model M-15, and sample analysis was done in a range of 400–4000 cm^{-1}. Differential Scanning Calorimeter (DSC) study was done PerkinElmer DSC 400 to obtain T_g of membranes; samples were studied in the range of 30–250 °C with N_2 flow of 20 ml min^{-1} and heating/cooling rate of 10 °C min^{-1}. Field Emission Scanning Electron Microscope characterization was done using the FESEM, FEI-ApreoLoVac model to obtain the morphology of MOFs and membranes. Brunauer–Emmett–Teller (BET) analysis was done to obtain the surface area, pore size, and pore volume of MOFs, using Quantachrome model-Autosorb iQ-C-XR *via* N_2 adsorption–desorption isotherms at 77 K. The characterized membranes are labelled M1-3 and I1-3, as mentioned in Table 1.

Gas permeation tests were conducted for all the prepared membranes, where the membrane was placed in between two rubber gaskets and then placed in a membrane testing module connected with a CO_2/CH_4 gas mixture. The schematic of the experimental setup was displayed with a detailed explanation in our previous paper.[29] Permeability of the gases (CO_2 and CH_4) and CO_2/CH_4 selectivity were calculated using eqn (2) and (3), respectively.

Table 1 Membrane sample codes

Membrane	Sample code
Pure PSF	PSF
2 wt% MIL-68(In)–NH_2/PSF	M1
10 wt% MIL-68(In)–NH_2/PSF	M2
20 wt% MIL-68(In)–NH_2/PSF	M3
2 wt% In(aip)$_2$/PSF	I1
10 wt% In(aip)$_2$/PSF	I2
20 wt% In(aip)$_2$/PSF	I3

$$P = \frac{Q \times l}{A \times \Delta p} \quad (2)$$

where Q is the permeate flow rate (cm^3 s^{-1}), l is the membrane thickness (in cm), A is the membrane area (in cm^2), Δp is the partial pressure difference of the gas species on the permeate and retentate side (in cm Hg).

Selectivity (α_{CO_2/CH_4}), no units is the ratio of permeabilities of CO_2 and CH_4.

$$\alpha_{CO_2/CH_4} = \frac{P_{CO_2}}{P_{CH_4}} \quad (3)$$

3 Results and discussion

3.1 Characterizations of MOFs and membranes

Fig. 2a shows the XRD graphs of the synthesized to MOFs MIL-68(In)–NH_2 and In(aip)$_2$, the 2θ peaks of MIL-68(In)–NH_2 at 4.7, 8.1, 9.3 16.3, 18.8 and additional peaks around 25, 26.3 shows typical MIL-68 structure which was reported in the literature.[30] XRD pattern of In(aip)$_2$ shows 2θ peaks around 6.9, 9.2, 9.7, 14.3, 16.04, 20.3, and 27.3, which corresponds to simulated peaks of typical 2D MOFs with 5-aminoisothaphilc acid linker from previous studies.[16,31] Also, we have done XRD for MOF samples (MIL-68(In)–NH_2 and In(aip)$_2$) to check their stability in chloroform solvent, and in Fig. S1,† we can see that there were no alterations in XRD peaks of MOFs. Fig. 2b shows the XRD patterns of prepared membranes, and the PSF membrane shows the broad peaks of 2theta around 19.5 and 29.6,[32,33] showing the amorphous nature of polymer after membrane fabrication. M1, M2, and M3 samples show an increase in sharpness peaks within the broad peaks with an increase in MOF wt%; similarly, for I1, I2, and I3 samples, sharp peaks intensity was increased as an increase in filler composition. This presence of sharp peaks within the broad peaks of PSF indicated the incorporation of MOF-fillers (MIL-68(In)–NH_2, In(aip)$_2$) in the polymer. In MMM samples, peak shifting was also observed, so we calculated intersegmental distance (d-spacing) using the Braggs equation.[34] PSF membrane's d-spacing of 0.45 nm was observed, and also for samples M1, M2, M3, I1, I2, and I3, d-spacing values were found to be 0.57 nm, 0.55 nm, 0.52 nm, 0.552 nm, 0.422 nm, and 0.423 nm respectively. This shift in the membranes' d-spacing indicates that crystallinity was added to amorphous polymeric membranes and that additional MOF fillers have settled in polymer chains (Fig. 2b).

Fig. 3a shows the FTIR spectra of the synthesized MOFs (MIL-68(In)–NH_2, In(aip)$_2$), FTIR of MIL-MOF shows peaks at

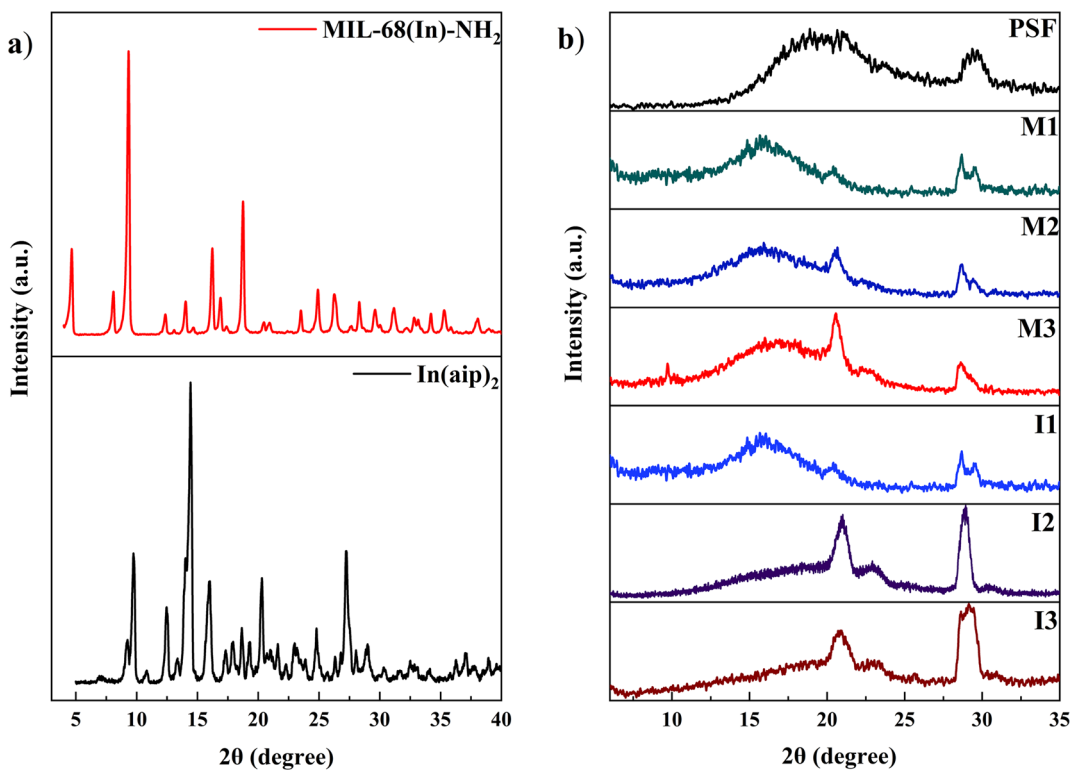

Fig. 2 XRD of (a) MOFs and (b) membranes.

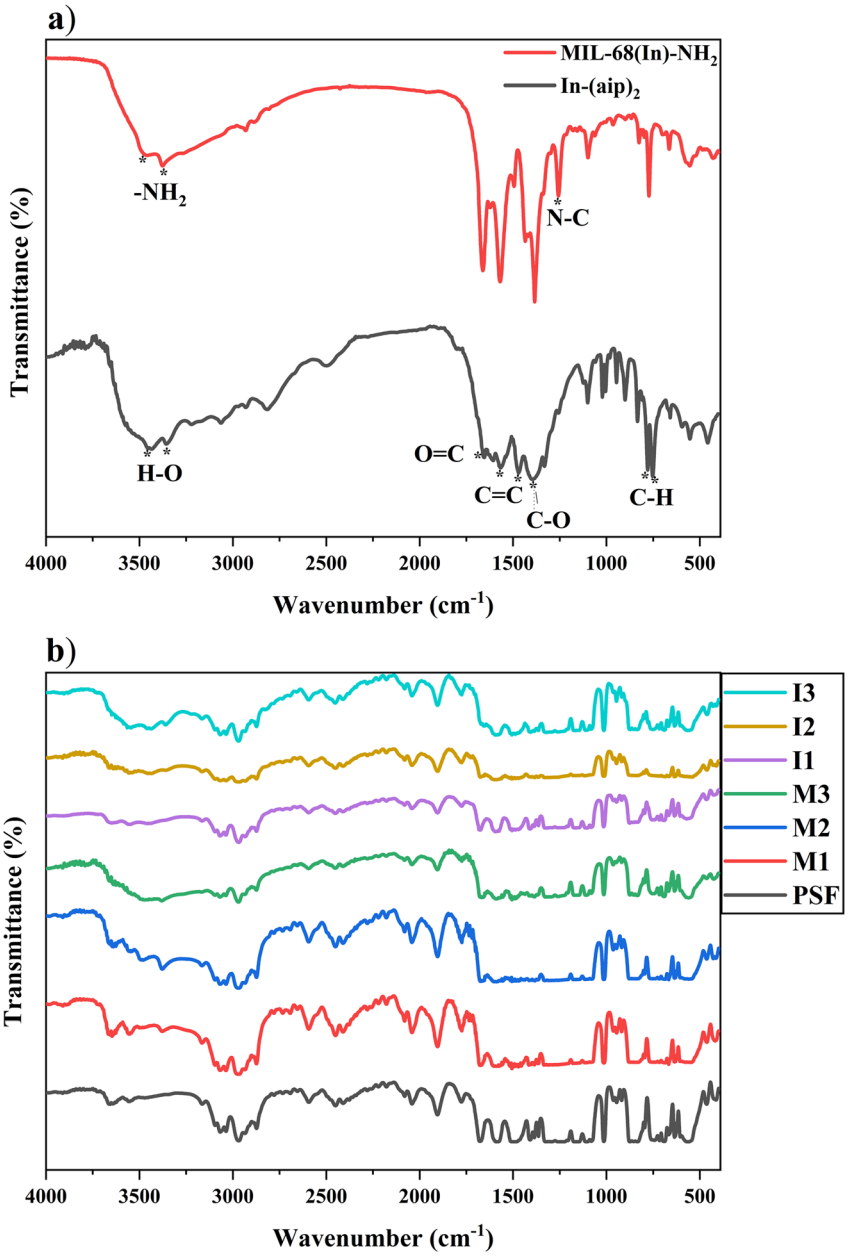

Fig. 3 FTIR of (a) MOFs and (b) membranes.

around 3490 cm^{-1} and 3367 cm^{-1} showing the presence of $-NH_2$ bond and peaks at 1256 cm^{-1} is due to presence of N–C bond.[13,35] $In(aip)_2$ MOFs FTIR spectra show the peaks for H–O stretching around 3455 cm^{-1} and 3352 cm^{-1}, C=O stretching at 1660 cm^{-1}, bending peaks of C=C were found at 1471 cm^{-1} and 1567 cm^{-1}, at 1398 cm^{-1} stretching peak of C–O was observed and at 750 cm^{-1} and 759 cm^{-1} stretching peaks of C–H bonds were obtained.[16] The FTIR spectra of membranes are shown in Fig. 3b; in all the membrane samples, we can observe the traditional peaks of polysulfone polymer. The C–H stretch peak in the benzene and CH_3–C bonds is seen at about 3000 cm^{-1}. The peaks at 1550 cm^{-1} show the complete benzene ring stretch, while the polysulfone polymer's SO_2 bond is represented by the peaks at around 1275 cm^{-1}. The SO_2 bond, which occasionally cannot be fully enhanced because of the overlap of C–C stretching, was identified as the source of the peaks at about 1275 cm^{-1}. The presence of peaks in all membranes indicates that the polysulfone polymer structure has not been damaged or disrupted during membrane formation. Also, no additional peaks or shifting of peaks were observed, indicating the settlement of filler particles (MIL-68(In)–NH_2/$In(aip)_2$) within the free volume of polymer present in between their chains. This also corresponds to the XRD results, where MMMs also showed broader peaks, suggesting the amorphous nature of polymers despite the sharp peaks of filler.

Fig. 4 shows the FESEM images of MIL-68(In)–NH_2 and $In(aip)_2$, which shows the clear difference between the two

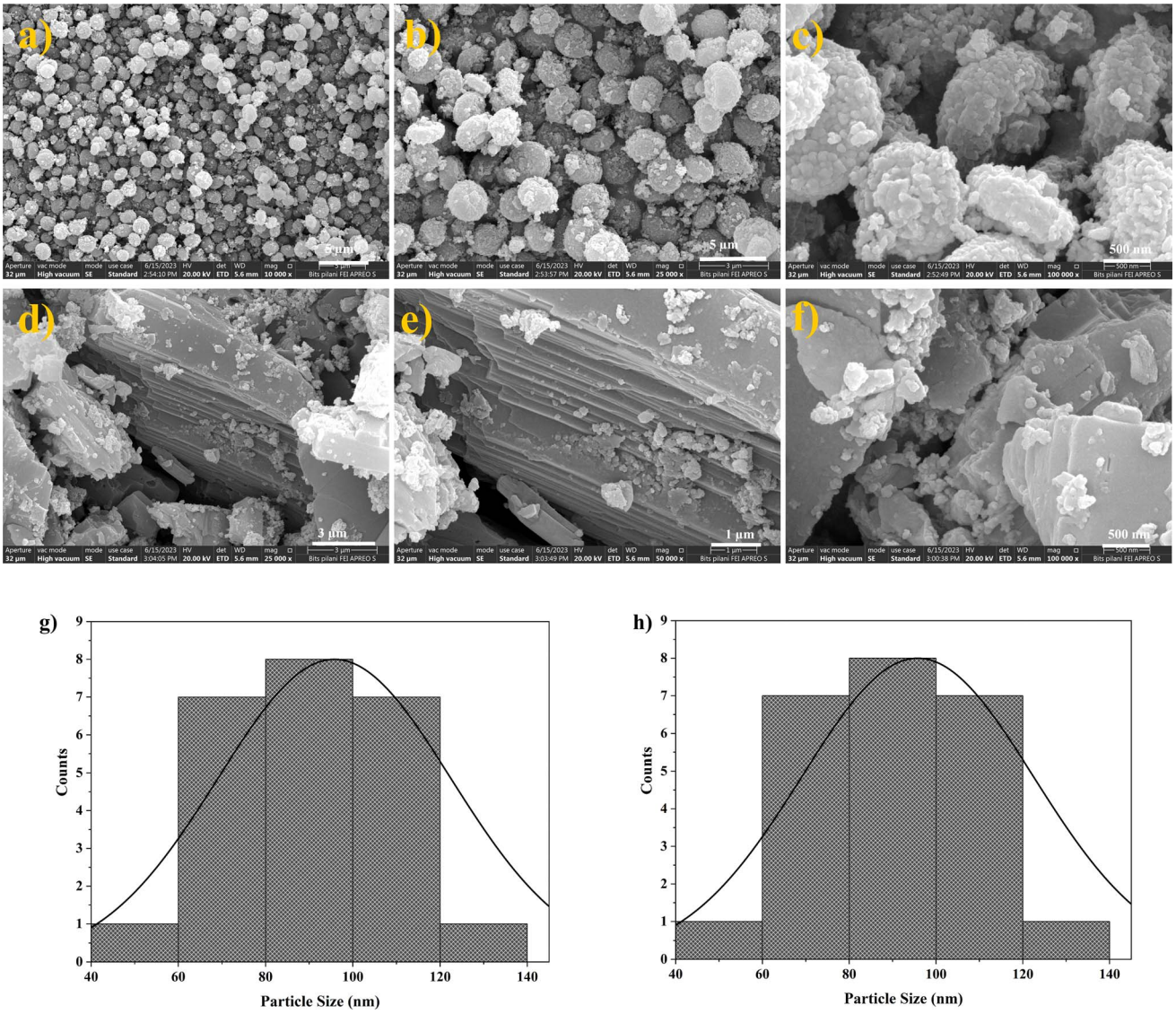

Fig. 4 FESEM images and particle size distribution of (a–c and g) MIL-68(In)–NH_2, (d–f and h) In(aip)$_2$.

MOFs. In Fig. 4a–c, we can see the FESEM images of MIL-68(In)–NH_2, and where the MOFs average particle size was observed as 95.8 nm in Fig. 4g (Image J software), particles are structure spherical in structure (3D). 2D layered (sheets) structure of In(aip)$_2$ MOF structure can be seen in Fig. 4d, e and f, and the average particle size of In(aip)$_2$ MOF was found to be 80 nm (Fig. 4h). Pure PSF membrane FESEM images were shown in a previous study.[28] Fig. 5 shows the top view and cross-section view of FESEM images of M1, M2, M3, I1, I2, and I3 membrane samples. Fig. 5a, d and g shows the top view of samples M1, M2, and M3, respectively, and we see that filler agglomeration increases as an increase in filler percentage and also observe that the no membrane samples have voids or pinholes. Similarly, the phenomena are observed in Fig. 5j, m and p (top view of samples I1, I2, and I3); we can see the filler dispersion of 2D MOF. In the cross-section images Fig. 5b, e, h, k, n and q of membrane samples, we can see that with the increase in the filler dispersion, the membrane's structure is altered slightly, which is indicated by the transformation of smooth and dense cross-section to rough. In Fig. 5c, f and i, we can see the distribution of filler particles MIL-68(In)–NH_2 have settled within the polymer without any void or pore formation. We can see the filler agglomerates in Fig. 5i (M3 sample). In(aip)$_2$ filler particle distribution can be observed in Fig. 5l, o and r; we can see that filler agglomerates are less compared to the M3 sample and also due to the 2D structure of filler (In(aip)$_2$), the dispersion of filler is not clearly visible in Fig. 5o and r (FESEM image of I2 and I3). In Fig. 5, we have not observed any membrane deformations or structure damage of PSF polymer with the addition of fillers, which corresponds to the XRD and FTIR results.[36]

The glass transition temperature (T_g) of membrane samples was obtained by DSC analysis and is given in Table 2. The T_g of the PSF membrane was found to be around 177 °C.[37] Compared to the PSF membrane, the T_g of M3 and I3 membrane samples rise to 184 °C and 183 °C, respectively, as the filler wt%

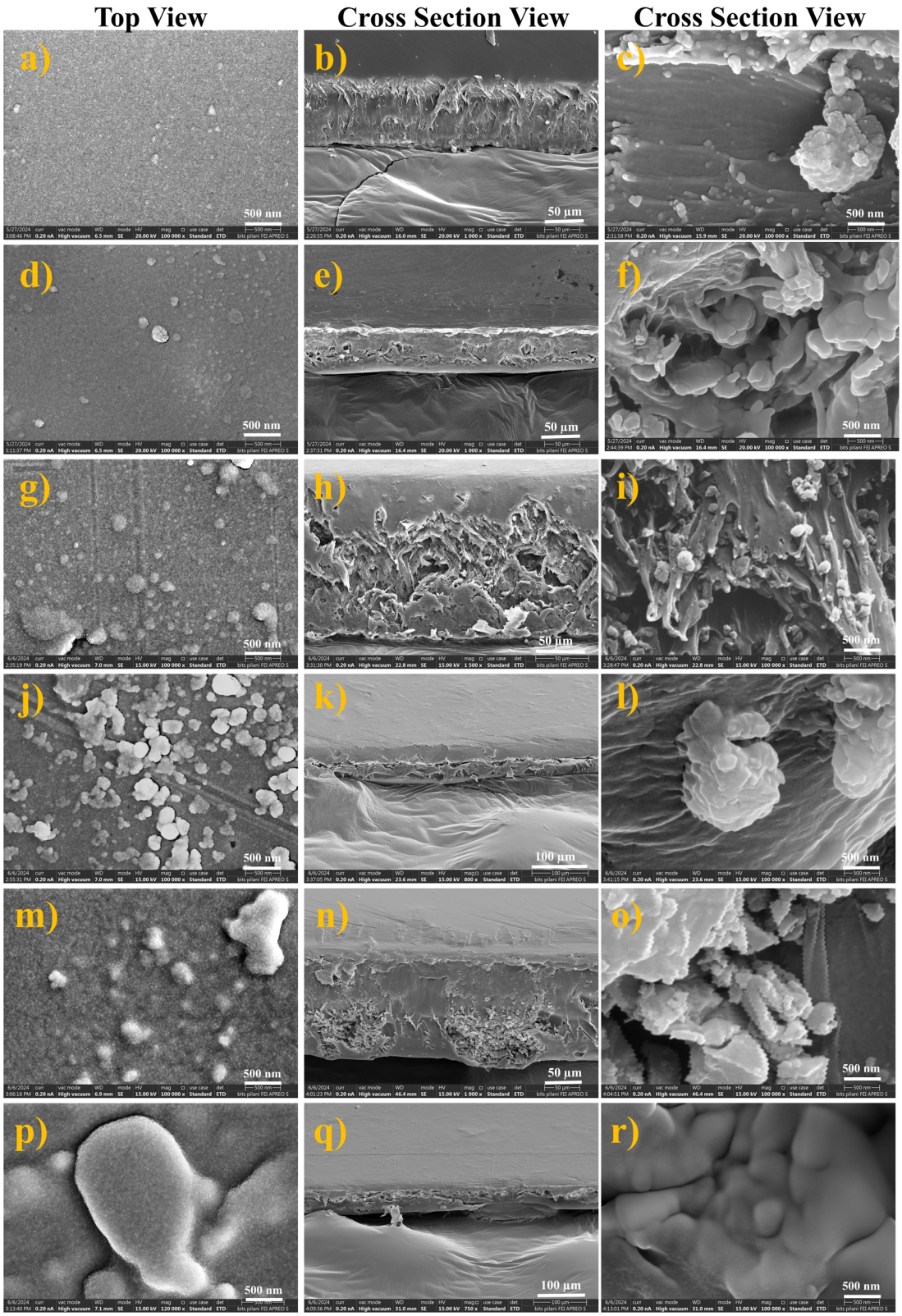

Fig. 5 FESEM images of membrane samples (a–c) M1, (d–f) M2, (g–i) M3, (j–l) I1, (m–o) I2, (p–r) I3.

increases. We can observe the increase in T_g by adding just 2 wt% of filler in M1 (179 °C) and I1 (178 °C) samples. This rise in the T_g shows the strong interactions between the filler particles (MIL-68(In)–NH_2 and $In(aip)_2$) and PSF polymer. Also, the increase in the T_g signifies rigidified zones in the filler–polymer interface. It indicates the increase in the crystallinity of

Table 2 T_g of membrane samples

Membrane sample	Glass transition temperature-T_g (°C)
PSF	177.6 ± 0.2
M1	179.8 ± 0.3
M2	181.8 ± 0.6
M3	184.2 ± 0.5
I1	178.4 ± 0.6
I2	180.9 ± 0.3
I3	183.2 ± 1.1

Table 3 BET measurements of MOFs

MOFs	BET surface area ($m^2\ g^{-1}$)	Pore volume ($cc\ g^{-1}$)	Pore size (nm)
MIL-68-(In)–NH_2	501.35	0.43	1.73
In(aip)$_2$	6.41	0.09	28.02

membranes, which has also been observed in the XRD spectra of MMMs.

Adsorption and desorption isotherms of MIL-68(In)–NH_2 and In(aip)$_2$ in Fig. S3† show that both MOFs have good uptake capacity in low-pressure regions.[13] In Table 3, we can see the BET measurements of both MOFs, the BET surface and pore volume of MIL-68(In)–NH_2 was found to be 501.35 $m^2\ g^{-1}$ and 0.43 $cc\ g^{-1}$ respectively. The surface area valve was lower compared to previous studies reported,[31,38] possibly due to synthesis parameter variations. In(aip)$_2$ BET surface area was found to be 6.41 $m^2\ g^{-1}$ and pore volume of 0.09 $cc\ g^{-1}$. Pore sizes of 1.73 nm (microporous) and 28.02 nm (mesoporous) were observed for MIL-68(In)–NH_2 and In(aip)2, respectively, with pore size distribution curves (Fig. S6†).

3.2 Gas permeation tests

Gas permeation experiments were conducted for all the prepared membranes (pure PSF, MIL-68(In)–NH_2/PSF In(aip)$_2$/PSF) at 0.5 bar pressure difference. PSF membrane's CO_2 permeability value obtained (6.3 Barrer) was similar to some of the previously mentioned studies.[39,40] The CO_2 permeabilities and CO_2/CH_4 selectivities at different filler wt% were given in Fig. 6(a and b). In Fig. 6a, we can see the CO_2 permeability of 2 wt% MIL-68(In)–NH_2/PSF MMM has increased more than three times up to 22 Barrer (at lower filler loading). The permeability of CO_2 has increased exponentially with the increase in filler wt%. At 20 wt% of filler loading, the highest CO_2 permeability of 79 Barrer was obtained for MIL-68(In)–NH_2-based MMMs. This increment in the CO_2 permeability for MIL-68(In)–NH_2/PSF MMMs was due to the increase in the tortuous path for the gases (which is provided by filler) and also the increase in porosity due to MOF microporous structure (as discussed in BET results). Similarly, In(aip)$_2$ MOF-based MMMs at lower filler loading (2 wt%), CO_2 permeability has increased to 69.2 Barrer, which is almost a 950% increment. The permeability valves have increased steadily until 15 wt% filler loading

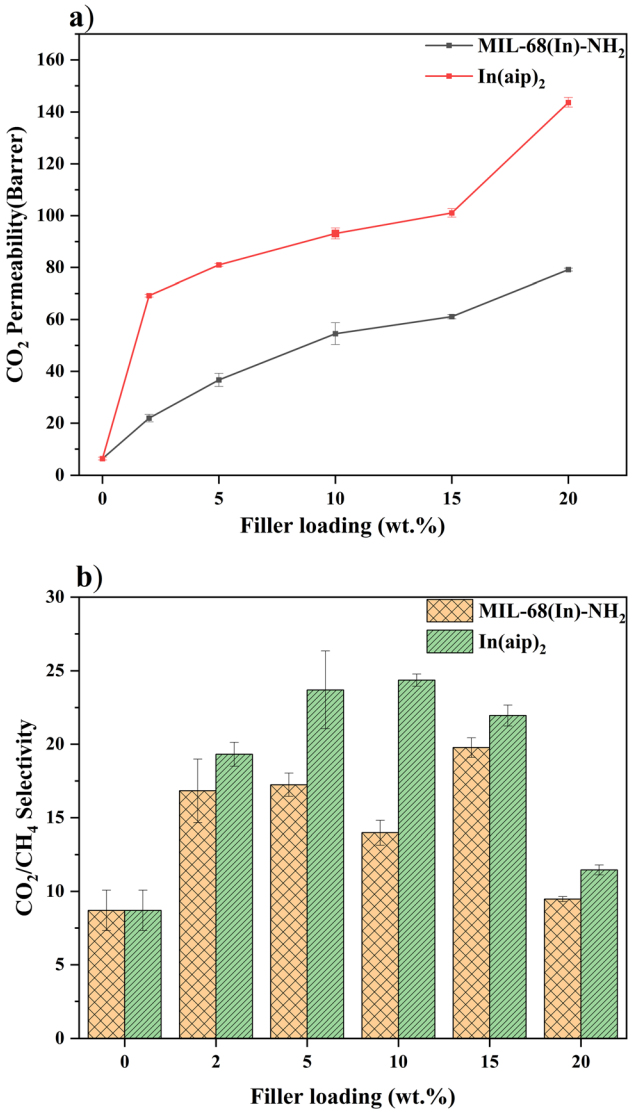

Fig. 6 (a) CO_2 permeabilities and (b) CO_2/CH_4 selectivities of pure PSF, MIL-68(In)–NH_2/PSF In(aip)$_2$/PSF membranes.

(101 Barrer). At 20 wt% of In(aip)$_2$, the highest CO_2 permeability of 144 Barrer was observed, which is almost 24 times more than the PSF membrane. The improvements in CO_2 permeability in both fillers-based MMMs can be attributed to the *d*-spacing shift, which creates more free spaces for CO_2 gas transport, and also, CO_2 has a faster diffusion rate in both MOFs at lower pressure.[39] The reasons for higher permeabilities for In(aip)$_2$/MMMs than MIL-68(In)–NH_2/MMMs are (1) due to its mesoporous nature (larger pore size from BET results), (2) the 2D nature of In(aip)$_2$ MOF the CO_2 and (3) high increase in T_g was observed (Table 2) for MIL-MOF based MMMs, which signifies the polymer rigidification restricting the CO_2 gas flow through the membrane.[41]

A comparison of CO_2/CH_4 selectivities for MIL-68(In)–NH_2/PSF MMMs and In(aip)2/PSF MMMs was given in Fig. 6b. The selectivities of MIL-58(In)–NH_2 and In(aip)$_2$ based MMMs have increased to 17 (95% increase) at 15 wt% loading and 24.4

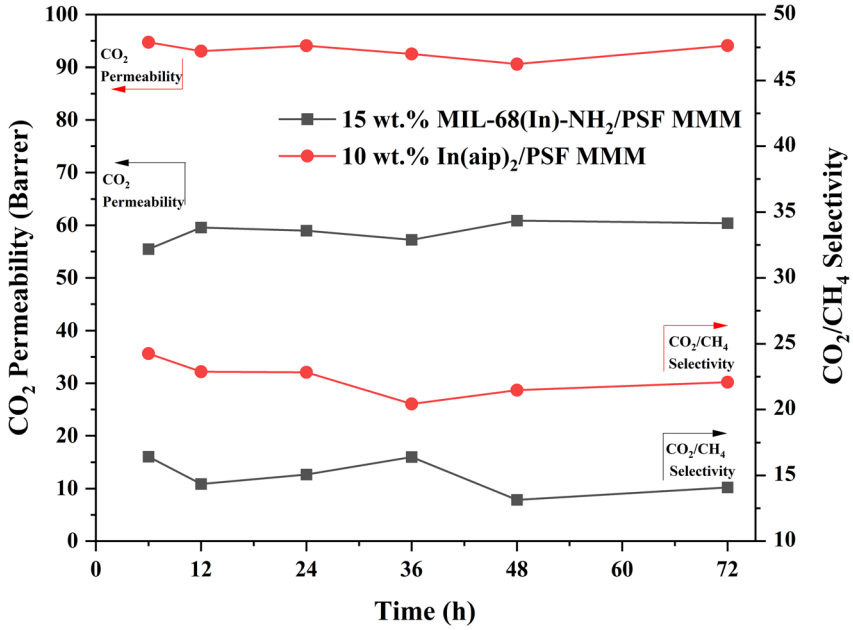

Fig. 7 Long term stability studies.

(180% increase) at 10 wt% loading, respectively, which are higher than PSF membrane (8.7). This increase in selectivities of CO_2/CH_4 for MIL-68(In)–NH_2-based MMMs is due to its high CO_2 uptake capacity at lower pressures[36] and also due to its uniform dispersion (in FESEM images) of filler, which allows more CO_2 than CH_4. In(aip)$_2$-based MMMs, enhanced selectivity can be attributed to its molecular sieving capacity (3.4–3.6 Å) and also due to its 2D-stacked structure, which provides Brønsted sites resulting in an increase of CO_2 affinity.[16,31] Two significant reasons for the rise in CO_2/CH_4 selectivities for both filler-based MMMs are the presence of hydrogen bonding, which allows extra sorption sites for CO_2 gas, and strong interactions of CO_2 molecules *via* carbonate zwitterion mechanism, due to the presence of amine (–NH_2) group in MOFs without causing hindrance to the structures.[15] The decrease in the CO_2/CH_4 selectivity at higher filler loadings is due to the agglomerates of MOFs formed in the membrane (FESEM image-Fig. 5i and r).[42,43] The gas separation mechanism of the MMMs prepared in study is due to synergistic effect of solution diffusion[44] (attributed to polymer matrix), tortuous path and CO_2 adsorption at lower pressure and temperature[13] (in the case of 3D MOF), and interlayer dispersion[45] and CO_2/CH_4 molecular sieving (in case of 2D MOF) as mentioned in Fig. 1a and b.

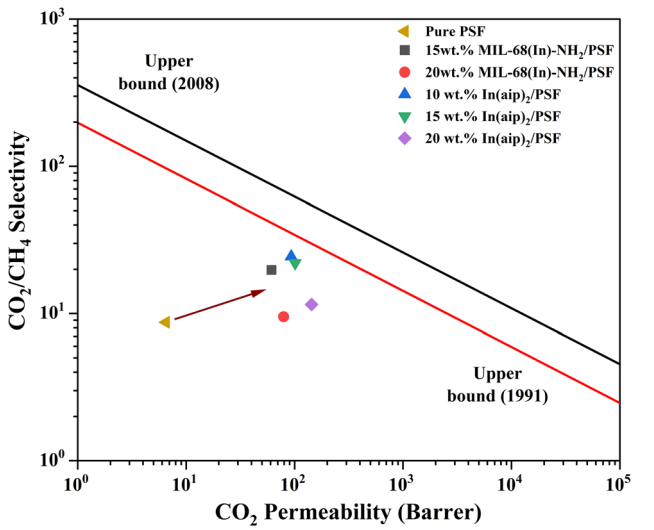

Fig. 8 Status of MIL-68(In)–NH_2, In(aip)$_2$ and PSF based MMMs on Robeson plot.

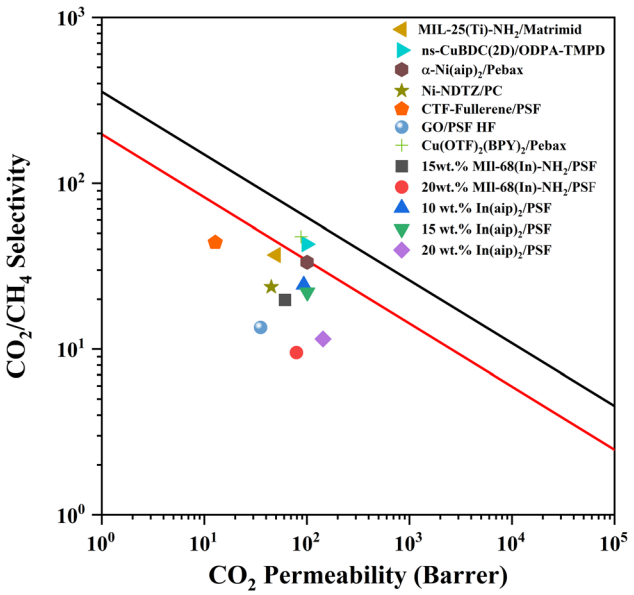

Fig. 9 Robeson's plot with literature comparison.

Table 4 Comparing the data from the literature and the gas permeation data of this study[a]

Membrane	Filler (wt%)	Testing conditions and feed mixture	P_{CO_2} (Barrer)	α_{CO_2/CH_4}	Reference
MIL-125(Ti)–NH_2/Matrimid	15	1 bar, 25 °C and pure gases	50	37	19
ns-CuBDC (2D)/ODPA–TMPD	2	1 bar, 25 °C and binary gas mixture	99	43	20
ZIF-8 (3D)/ODPA–TMPD	10	1 bar, 25 °C and binary gas mixture	144	37	20
α-Ni$(aip)_2$/Pebax	2	2 bar, 25 °C and binary gas mixture	100.6	33.4	21
Ni-NDTZ/PC	20	30 °C and pure gases	45	23.7	23
N-GO/PI	0.02	3 bar, 25 °C and pure gases	28*	47	24
CTF-fullerene/PSF	24	3 bar, 25 °C and binary gas mixture	17.8	30	25
CTF-fullerene/Matrimid	24	3 bar, 25 °C and binary gas mixture	12.8	44	25
IL@SAPO-34/PSF	5	2.75 bar, 25 °C and pure gases	7.24*	20.4	26
NH_2-ZIF-8/PSF	15	1.5 bar, 25 °C and 60 : 40-CH_4 : CO_2	21	14	28
UiO-66-NH_2@ICA/Matrimid	10	3 bar, 25 °C and binary gas mixture	40.1	64.7	48
GO/PSF HF	0.25	1 bar, 25 °C and binary gas mixture	35.4	13.5	49
$Cu(OTF)_2(BPY)_2$/Pebax	4	25 °C and pure gases	87.6	47.6	50
MIL-68(In)–NH_2/PSF	15	1.5 bar, 25 °C and 60 : 40-CH_4 : CO_2	61.2	19.8	This work
MIL-68(In)–NH_2/PSF	20	1.5 bar, 25 °C and 60 : 40-CH_4 : CO_2	79.2	9.5	This work
In$(aip)_2$/PSF	10	1.5 bar, 25 °C and 60 : 40-CH_4 : CO_2	93.1	24.4	This work
In$(aip)_2$/PSF	15	1.5 bar, 25 °C and 60 : 40-CH_4 : CO_2	101.1	22	This work
In$(aip)_2$/PSF	20	1.5 bar, 25 °C and 60 : 40-CH_4 : CO_2	143.7	11.5	This work

[a] HF-hollow fibers, *GPU.

To assess the commercial applications of our prepared membrane, long-term stability studies have been conducted for two membranes 15 wt% MIL-68(In)–NH_2/PSF MMM and 10 wt% In$(aip)_2$/PSF MMM due to their high CO_2 selective performance. Each sample was tested by performing a 72 hour run with a gas permeation setup, and sampling was done at 6 h, 12 h, 24 h, 36 h, 48 h, and 72 h. Fig. 7 shows the plot for long-term stability time *vs.* CO_2 permeability and CO_2/CH_4 selectivity. The findings of this study show that both CO_2 permeability and CO_2/CH_4 selectivity have remained stable throughout the 72 h run time, and remained within the standard deviation of values as given in Fig. 6. These results show that the membrane's CO_2 plasticization and good membrane stability are not affected during long (continuous) operations.

3.3 Literature comparison

In Fig. 8 we can see prepared membrane's separation performance using Robeson upper bounds (1991 and 2001)[46,47] and in Fig. 9 we can see Robeson plot with prepared membranes in this study and some other studies reported in literature. In Robeson plot, we can see that MMMs in this study when compared to pure PSF membrane are moving towards upper bond as represented in Fig. 7. Unlike some other studies[23,28,29,42] which have not progressed towards the Robeson upper bounds. The prepared membranes' performance is also evaluated by comparing with some of the studies discussed in the earlier section[19–21,23–26,28] and other available studies in Table 4. The UiO-66-NH_2 MOF has been grafter with imidazole-2-carbaldehyde (ICA) (UiO-66-NH_2@ICA) and dispersed in Matrimid polymer. Due to an increase in the pore volume of filler at 10 wt% of UiO-66-NH_2@ICA in Matrimid, CO_2 permeability and CO_2/CH_4 selectivity of 40.1 and 64.7 were obtained, respectively.[48] Polysulfone-based hollow fibers were fabricated with GO-nanosheets as filler due to their oxygen abundance and their hydrophilic nature to attract gases. At 0.25 wt% of filler in PSF and with mixed gas used for testing, the CO_2 permeability was found to be 35.4, and 13.4 of CO_2/CH_4 selectivity was obtained.[49] Copper-based 2D MOF ($Cu(OTF)_2(BPY)_2$) (OTF = $CF_3SO_3^-$ and BPY = 4,4′-bipyridine) was synthesized as filler to provide interlaminate channels for CO_2 gas, and MMMs were fabricated by $Cu(OTF)_2(BPY)_2$ dispersing in Pebax polymer. At 4 wt% of filler content, CO_2 permeability of 86.7 Barrer and CO_2/CH_4 selectivity of 47.6 was observed.[50]

Table 4 and Fig. 9 shows that the CO_2 permeabilities of the MMMs prepared in this study have surpassed some of the literature[19–21,23,25,28,48–50] mentioned above. Also, CO_2/CH_4 selectivities obtained are higher than in some studies.[26,28,49] The comparison studies show that the 2D filler-based MMMs have performed better than 3D filler-based MMMs in terms of CO_2/CH_4 separation, making In$(aip)_2$ an effective filler for gas separation.

4 Conclusion

This paper demonstrates the preparation of PSF-based MMMs with MIL-68(In)–NH_2, In$(aip)_2$ as fillers for CO_2/CH_4 mixed gas separation. XRD, FTIR, FESEM, and BET filler analysis have shown MOFs' crystalline and porous nature. XRD of MMMs has shown a shift in *d*-spacing, indicating the settlement of filler in the polymer, which their FTIR spectra backing up. The shift of T_g in membranes was observed in DSC analysis, showing a good interaction between MOFs and the polymer. FESEM images of MMMs showed good dispersion of fillers in the PSF matrix at lower loadings and agglomerations at higher loadings. Fabricated MMMs have improved CO_2 gas separation in terms of CO_2 permeability and CO_2/CH_4 selectivity. Compared to pure PSF membrane permeability of CO_2 increment of 1150% (MIL-68(In)–NH_2) and 2180% (In$(aip)_2$) for 20 wt% filler loading. Highest CO_2/CH_4 selectivities of 19.8 for 15 wt% MIL-68(In)–

NH_2/PSF MMM and 24.4 for $In(aip)_2$/PSF MMM. A literature comparison was made for gas permeation data obtained, which showed the superior CO_2 separation performance of the membranes prepared in this study. Overall, this work shows the potential of indium (In) based MOFs as fillers in membranes for other gas separations, which can be explored in future studies.

Data availability

The authors declare that the data supporting the findings of this study are available within the paper.

Author contributions

Aditya Jonnalagedda (AJ): conceptualization, methodology, investigation, data curation, writing – original draft; Bhanu Vardhan Reddy Kuncharam (BVRK): conceptualization, methodology, formal analysis, visualization, writing – review & editing, funding acquisition, supervision.

Conflicts of interest

There are no conflicts to declare.

Acknowledgements

The work is funded by the Department of Science and Technology (DST)-Science and Engineering Research Board (SERB), MTR/2023/000355. Principal Investigator: Bhanu Vardhan Reddy Kuncharam.

References

1 T. L. Frölicher, M. Winton and J. L. Sarmiento, *Nat. Clim. Change*, 2014, **4**, 40–44.
2 A. Ç. Köne and T. Büke, *Renewable Sustainable Energy Rev.*, 2010, **14**, 2906–2915.
3 V. Vasan, N. V. Sridharan, M. Feroskhan, S. Vaithiyanathan, B. Subramanian, P.-C. Tsai, Y.-C. Lin, C.-H. Lay, C.-T. Wang and V. K. Ponnusamy, *Process Saf. Environ. Prot.*, 2024, **186**, 518–539.
4 P. Abdeshahian, J. S. Lim, W. S. Ho, H. Hashim and C. T. Lee, *Renewable Sustainable Energy Rev.*, 2016, **60**, 714–723.
5 R. Khalilpour, K. Mumford, H. Zhai, A. Abbas, G. Stevens and E. S. Rubin, *J. Cleaner Prod.*, 2015, **103**, 286–300.
6 D. F. Sanders, Z. P. Smith, R. Guo, L. M. Robeson, J. E. McGrath, D. R. Paul and B. D. Freeman, *Polymer*, 2013, **54**, 4729–4761.
7 P. Tanvidkar, S. Appari and B. V. R. Kuncharam, *Rev. Environ. Sci. Biotechnol.*, 2022, **21**, 539–569.
8 W. Fan, Y. Ying, S. B. Peh, H. Yuan, Z. Yang, Y. Di Yuan, D. Shi, X. Yu, C. Kang and D. Zhao, *J. Am. Chem. Soc.*, 2021, **143**, 17716–17723.
9 J. Deng, Z. Huang, B. J. Sundell, D. J. Harrigan, S. A. Sharber, K. Zhang, R. Guo and M. Galizia, *Polymer*, 2021, **229**, 123988.
10 M. M. Lichaei and J. Thibault, *Process Saf. Environ. Prot.*, 2024, **183**, 952–975.
11 F. Serpaggi, T. Loiseau, F. Taulelle and G. Férey, *Microporous Mesoporous Mater.*, 1998, **20**, 197–206.
12 B. E. Keshta, H. Yu and L. Wang, *Sep. Purif. Technol.*, 2023, **322**, 124301.
13 L. Wu, M. Xue, S.-L. Qiu, G. Chaplais, A. Simon-Masseron and J. Patarin, *Microporous Mesoporous Mater.*, 2012, **157**, 75–81.
14 R. Liang, L. Shen, F. Jing, W. Wu, N. Qin, R. Lin and L. Wu, *Appl. Catal., B*, 2015, **162**, 245–251.
15 B. Arstad, H. Fjellvåg, K. O. Kongshaug, O. Swang and R. Blom, *Adsorption*, 2008, **14**, 755–762.
16 Y.-M. Gu, H.-F. Qi, S. Qadir, T.-J. Sun, R. Wei, S.-S. Zhao, X.-W. Liu, Z. Lai and S.-D. Wang, *Chem. Eng. J.*, 2022, **449**, 137768.
17 Y. Wang, M. Fu, S. Zhou, H. Liu, X. Wang, W. Fan, Z. Liu, Z. Wang, D. Li, H. Hao, X. Lu, S. Hu and D. Sun, *Chem*, 2022, **8**, 3263–3274.
18 W. Fan, S. Yuan, W. Wang, L. Feng, X. Liu, X. Zhang, X. Wang, Z. Kang, F. Dai, D. Yuan, D. Sun and H. C. Zhou, *J. Am. Chem. Soc.*, 2020, **142**, 8728–8737.
19 M. Waqas Anjum, B. Bueken, D. De Vos and I. F. J. Vankelecom, *J. Membr. Sci.*, 2016, **502**, 21–28.
20 S. A. S. C. Samarasinghe, C. Y. Chuah, Y. Yang and T.-H. Bae, *J. Membr. Sci.*, 2018, **557**, 30–37.
21 C. Li, C. Wu and B. Zhang, *ACS Sustain. Chem. Eng.*, 2020, **8**, 642–648.
22 E. G. Ajebe, C.-C. Hu, C.-F. Wang, W.-S. Hung, H.-C. Tsai, N. K. Hundessa, K.-R. Lee and J.-Y. Lai, *Mater. Today Sustain.*, 2024, **26**, 100818.
23 A. Valverde-Gonzalez, N. Yuriychuk, M. C. Borrallo-Aniceto, F. Gándara, M. Iglesias, M. López-González and E. M. Maya, *ACS Appl. Polym. Mater.*, 2024, **6**, 4244–4255.
24 M. Aghajohari, H. Fazeli-Khosh, M. Adibi and A. Sharif, *ACS Appl. Polym. Mater.*, 2024, **6**, 2576–2585.
25 S. Bügel, A. Spieß and C. Janiak, *Microporous Mesoporous Mater.*, 2021, **316**, 110941.
26 N. N. R. Ahmad, C. P. Leo, A. W. Mohammad and A. L. Ahmad, *Microporous Mesoporous Mater.*, 2017, **244**, 21–30.
27 S. Yousef, A. Tonkonogovas, V. Makarevicius and A. Mohamed, *Chemosphere*, 2024, **358**, 142166.
28 A. Jonnalagedda and B. V. R. Kuncharam, *J. Appl. Polym. Sci.*, 2023, **140**, e54650.
29 P. Tanvidkar, A. Jonnalagedda and B. V. R. Kuncharam, *J. Appl. Polym. Sci.*, 2023, **140**, e53264.
30 C. Volkringer, M. Meddouri, T. Loiseau, N. Guillou, J. Marrot, G. Férey, M. Haouas, F. Taulelle, N. Audebrand and M. Latroche, *Inorg. Chem.*, 2008, **47**, 11892–11901.
31 R.-B. Lin, L. Li, A. Alsalme and B. Chen, *Small Struct.*, 2020, **1**, 1–5.
32 S. Rabiej, B. Ostrowska-Gumkowska and A. Włochowicz, *Eur. Polym. J.*, 1997, **33**, 1031–1039.
33 M. Farrokhara and F. Dorosti, *Chin. J. Chem. Eng.*, 2020, **28**, 2301–2311.
34 B. Nayak, P. Tanvidkar and B. V. R. Kuncharam, *Polym. Eng. Sci.*, 2023, **64**, 788–797.

35 T. Ahnfeldt, D. Gunzelmann, T. Loiseau, D. Hirsemann, J. Senker, G. Férey and N. Stock, *Inorg. Chem.*, 2009, **48**, 3057–3064.
36 A. Jonnalagedda and B. V. R. Kuncharam, *RSC Adv.*, 2024, **14**, 27074–27085.
37 H. Abdul Mannan, H. Mukhtar, M. Shima Shaharun, M. Roslee Othman and T. Murugesan, *J. Appl. Polym. Sci.*, 2016, **133**, 1–9.
38 Y.-H. Li, S.-L. Wang, Y.-C. Su, B.-T. Ko, C.-Y. Tsai and C.-H. Lin, *Dalton Trans.*, 2018, **47**, 9474–9481.
39 B. Zornoza, A. Martinez-Joaristi, P. Serra-Crespo, C. Tellez, J. Coronas, J. Gascon and F. Kapteijn, *Chem. Commun.*, 2011, **47**, 9522–9524.
40 X. Guo, H. Huang, Y. Ban, Q. Yang, Y. Xiao, Y. Li, W. Yang and C. Zhong, *J. Membr. Sci.*, 2015, **478**, 130–139.
41 C. L. Lee, H. L. Chapman, M. E. Cifuentes, K. M. Lee, L. D. Merrill, K. L. Ulman and K. Venkataraman, *J. Membr. Sci.*, 1988, **38**, 55–70.
42 P. Tanvidkar, A. Jonnalagedda and B. V. R. Kuncharam, *Environ. Technol.*, 2024, **45**, 2867–2878.
43 A. Car, C. Stropnik and K. V. Peinemann, *Desalination*, 2006, **200**, 424–426.
44 M. Z. Ahmad, V. Martin-Gil, V. Perfilov, P. Sysel and V. Fila, *Sep. Purif. Technol.*, 2018, **207**, 523–534.
45 K. Duan, J. Wang, Y. Zhang and J. Liu, *J. Membr. Sci.*, 2019, **572**, 588–595.
46 L. M. Robeson, *J. Membr. Sci.*, 1991, **62**, 165–185.
47 L. M. Robeson, *J. Membr. Sci.*, 2008, **320**, 390–400.
48 Y. Jiang, C. Liu, J. Caro and A. Huang, *Microporous Mesoporous Mater.*, 2019, **274**, 203–211.
49 K. Sainath, A. Modi and J. Bellare, *Chem. Eng. J. Adv.*, 2021, **5**, 100074.
50 M. Gou, W. Zhu, Y. Sun and R. Guo, *Sep. Purif. Technol.*, 2021, **259**, 118107.